San Jose State University

From the SelectedWorks of Aaron J. Romanowsky

2016

Discovery of the Candidate Off-Nuclear Ultrasoft Hyper-Luminous X-Ray Source 3XMM J141711.1+522541

Dacheng Lin, *University of New Hampshire, Durham*
Eleazar R. Carrasco, *Gemini Observatory/AURA, Southern Operations Center*
Natalie A. Webb, *CNRS*
Jimmy A. Irwin, *University of Alabama - Tuscaloosa*
Renato Dupke, *University of Alabama - Tuscaloosa*, et al.

Available at: https://works.bepress.com/aaron_romanowsky/109/

The Astrophysical Journal, 821:25 (12pp), 2016 April 10 doi:10.3847/0004-637X/821/1/25
© 2016. The American Astronomical Society. All rights reserved.

DISCOVERY OF THE CANDIDATE OFF-NUCLEAR ULTRASOFT HYPER-LUMINOUS X-RAY SOURCE 3XMM J141711.1+522541

Dacheng Lin[1], Eleazar R. Carrasco[2], Natalie A. Webb[3,4], Jimmy A. Irwin[5], Renato Dupke[5,6,7,8], Aaron J. Romanowsky[9,10], Enrico Ramirez-Ruiz[11], Jay Strader[12], Jeroen Homan[13,14], Didier Barret[3,4], and Olivier Godet[3,4]

[1] Space Science Center, University of New Hampshire, Durham, NH 03824, USA; dacheng.lin@unh.edu
[2] Gemini Observatory/AURA, Southern Operations Center, Casilla 603, La Serena, Chile
[3] CNRS, IRAP, 9 avenue du Colonel Roche, BP 44346, F-31028 Toulouse Cedex 4, France
[4] Université de Toulouse, UPS-OMP, IRAP, Toulouse, France
[5] Department of Physics and Astronomy, University of Alabama, Box 870324, Tuscaloosa, AL 35487, USA
[6] Observatório Nacional, Rua Gal. José Cristino 77, São Cristóvão, CEP20921-400 Rio de Janeiro RJ, Brazil
[7] Department of Astronomy, University of Michigan, 500 Church St., Ann Arbor, MI 48109, USA
[8] Eureka Scientific Inc., 2452 Delmer St. Suite 100, Oakland, CA 94602, USA
[9] Department of Physics and Astronomy, San José State University, One Washington Square, San José, CA 95192, USA
[10] University of California Observatories, 1156 High Street, Santa Cruz, CA 95064, USA
[11] Department of Astronomy and Astrophysics, University of California, Santa Cruz, CA 95064, USA
[12] Department of Physics and Astronomy, Michigan State University, East Lansing, Michigan, MI 48824, USA
[13] MIT Kavli Institute for Astrophysics and Space Research, MIT, 70 Vassar Street, Cambridge, MA 02139-4307, USA
[14] SRON, Netherlands Institute for Space Research, Sorbonnelaan 2, 3584 CA Utrecht, The Netherlands
Received 2015 December 25; accepted 2016 February 23; published 2016 April 5

ABSTRACT

We report the discovery of an off-nuclear ultrasoft hyper-luminous X-ray source candidate 3XMM J141711.1+522541 in the inactive S0 galaxy SDSS J141711.07+522540.8 ($z = 0.41827$, $d_L = 2.3$ Gpc) in the Extended Groth Strip. It is located at a projected offset of $\sim 1\farcs0$ (5.2 kpc) from the nucleus of the galaxy and was serendipitously detected in five *XMM-Newton* observations in 2000 July. Two observations have enough counts and can be fitted with a standard thermal disk with an apparent inner disk temperature $kT_{\rm MCD} \sim 0.13$ keV and a 0.28–14.2 keV unabsorbed luminosity $L_{\rm X} \sim 4 \times 10^{43}$ erg s^{-1} in the source rest frame. The source was still detected in three *Chandra* observations in 2002 August, with similarly ultrasoft but fainter spectra ($kT_{\rm MCD} \sim 0.17$ keV, $L_{\rm X} \sim 0.5 \times 10^{43}$ erg s^{-1}). It was not detected in later observations, including two by *Chandra* in 2005 October, one by *XMM-Newton* in 2014 January, and two by *Chandra* in 2014 September–October, implying a long-term flux variation factor of >14. Therefore the source could be a transient with an outburst in 2000–2002. It has a faint optical counterpart candidate, with apparent magnitudes of $m_{\rm F606W} = 26.3$ AB mag and $m_{\rm F814W} = 25.5$ AB mag in 2004 December (implying an absolute *V*-band magnitude of ~ -15.9 AB mag). We discuss various explanations for the source and find that it is best explained as a massive black hole (BH) embedded in the nucleus of a possibly stripped satellite galaxy, with the X-ray outburst due to tidal disruption of a surrounding star by the BH. The BH mass is $\sim 10^5\,M_\odot$, assuming the peak X-ray luminosity at around the Eddington limit.

Key words: accretion, accretion disks – galaxies: individual: (3XMM J141711.1+522541) – galaxies: nuclei – X-rays: galaxies

1. INTRODUCTION

Optical dynamical measurements have confirmed the existence of stellar-mass black holes (BHs, $\sim 10\,M_\odot$) in some Galactic X-ray binaries (McClintock & Remillard 2006; Remillard & McClintock 2006) and supermassive BHs (SMBHs; $\sim 10^{5-10}\,M_\odot$) in the centers of massive galaxies (Kormendy & Richstone 1995). Most Galactic BH X-ray binaries are discovered when they experience transient outbursts. Many SMBHs are detected as active galactic nuclei (AGNs), while quiescent SMBHs can reveal themselves temporarily through tidal disruption of surrounding stars (Lidskii & Ozernoi 1979; Rees 1988, 1990). A few tens of tidal disruption event (TDE) candidates have been discovered in various wavelengths, with about twenty in X-rays (Komossa 2012, 2015). Their positions, at least for the X-ray candidates, are all consistent with emanating from the nuclei of their candidate host galaxies.

Off-nuclear/wandering massive BHs, including intermediate-mass BHs (IMBHs, $\sim 10^2$–$10^5\,M_\odot$) and SMBHs, have been predicted to exist through several important astrophysical processes. The processes for forming wandering IMBHs include, e.g., the collapse of massive population III stars in the early universe (e.g., Madau & Rees 2001); runaway merging of massive stars in young compact star clusters (e.g., Ebisuzaki et al. 2001; Gürkan et al. 2004); and accretion of a large amount of gas lost by the first generation of giant stars in the center of globular clusters (e.g., Vesperini et al. 2010). Given that galaxy merging is ubiquitous and that many dwarf galaxies with optical or X-ray signatures of nuclear massive BHs have been discovered (Reines et al. 2011, 2013; Maksym et al. 2013, 2014; Donato et al. 2014; Baldassare et al. 2015; Lemons et al. 2015), tidal stripping of merging satellite dwarf galaxies might result in wandering IMBHs or SMBHs (e.g., Islam et al. 2003; Bellovary et al. 2010). A SMBH of mass $\sim 2.1 \times 10^7\,M_\odot$ has been found in one of the brightest ultracompact dwarf galaxies (UCDs) yet known, i.e., UCD1 in M60, and many less massive UCDs were suggested as also containing wandering massive BHs (Seth et al. 2014). Wandering massive BHs embedded in compact stellar clusters can be revealed in several ways, such as accreting mass from a stellar

companian or tidal disruption of surrounding stars (Baumgardt et al. 2004, 2006; Hopman et al. 2004; Ramirez-Ruiz & Rosswog 2009; Stone & Loeb 2012; Liu & Chen 2013; MacLeod et al. 2014, 2015).

Many ultra-luminous X-ray sources (ULXs, see Feng & Soria 2011 for a review), which are off-nuclear point sources reaching $L_X > 10^{39}$ erg s^{-1} (the Eddington limit for a stellar-mass BH of $\sim$10 $M_\odot$), have been detected within nearby galaxies. However, most ULXs are still not luminous enough to be unambiguously associated with massive BHs; the beaming effect and/or super-Eddington accretion rates onto stellar-mass BHs can explain luminosities up to $\sim 10^{41}$ erg s^{-1} (e.g., Poutanen et al. 2007). With dynamical measurements of the masses of the BHs in two ULXs (Liu et al. 2013; Motch et al. 2014), detection of two transient ULXs in M31 showing transition from the super-Eddington state to standard spectral states of Galactic BH X-ray binaries (Middleton et al. 2012, 2013), and the confirmation of the ubiquitous curved spectra at high energy in the ULX spectra by *NuSTAR* (e.g., Bachetti et al. 2013; Walton et al. 2014), most ULXs are now believed to be super-Eddington accreting stellar-mass BHs. Bachetti et al. (2014) even found a ULX (M82 X-2) powered by an accreting neutron star.

In contrast, hyper-luminous X-ray sources (HLXs, $L_X > 10^{41}$ erg s^{-1}) are difficult to explain as stellar-mass BHs with beaming effects and/or super-Eddington accretion rates and are good targets to search for wandering massive BHs. ESO 243-49 HLX-1 is the most luminous HLX yet detected, with peak luminosity $L_X \sim 10^{42}$ erg s^{-1} and thermal disk temperatures of $<$0.3 keV, and has been argued to be an IMBH of $\sim 10^4 M_\odot$ (e.g., Farrell et al. 2009; Servillat et al. 2011; Godet et al. 2012; Webb et al. 2012). There are a dozen other HLX candidates, which have lower luminosities and hard X-ray spectra and are mostly persistent with flux variation factors of a few (e.g., Sutton et al. 2012). Some of them were shown to be background AGNs (e.g., Sutton et al. 2012, 2015). Some of the others show special properties distinguishing them from AGNs and are good HLX candidates hosting massive BHs (e.g., M82 X-1, with twin X-ray quasi-periodic oscillations, Pasham et al. 2014; CXO J122518.6 +144545, with possible recurrent outbursts, Heida et al. 2015).

In our continuing effort to classify X-ray sources serendipitously detected by *XMM-Newton* and *Chandra* (e.g., Lin et al. 2012, 2014), we discovered a possibly transient ultrasoft X-ray source 3XMM J141711.1+522541 (XJ1417+52 hereafter) in the *XMM-Newton* Serendipitous Source Catalog (the 3XMM-DR5 version, Rosen et al. 2015). The source was serendipitously detected in deep *XMM-Newton* and *Chandra* observations of the Extended Groth Strip (EGS, e.g., Laird et al. 2009) in 2000–2002. We ruled it out as an AGN in Lin et al. (2012) based on the ultrasoft X-ray spectra. In this paper, we report the properties of this source and argue that it is probably a wandering BH of mass $\sim 10^5 M_\odot$ embedded in a compact stellar cluster at a redshift of $z = 0.41827$ (the source luminosity distance is $d_L = 2.3$ Gpc, assuming a flat universe with $H_0 = 70$ km s^{-1} Mpc^{-1} and $\Omega_M = 0.3$), with the outburst due to disruption of a surrounding star. In Section 2, we describe the analysis of multiwavelength data. In Section 3, we first identify the host galaxy of our source and the optical counterpart, followed by the presentation of its detailed X-ray spectral and variability properties. We discuss the nature of our source in Section 4 and give the conclusions of our study in Section 5.

2. DATA ANALYSIS

2.1. XMM-Newton Observations

There were five *XMM-Newton* observations during 2000 July 20–24 that covered XJ1417+52 at off-axis angles of about 3.′4. We analyzed all of them and found that only two have enough counts from clean exposures for careful spectral modeling; they are referred to as X1 and X2 (Table 1). The other three (observation IDs: 127920401, 0127920901, and 0127921101) have clean exposure times of $<$10 ks after high background filtering (see below) and have $<$10 net counts in each European Photon Imaging Cameras (EPICs) camera. We will not present these observations further in this study, but we note that the source was detected in these observations, with fluxes consistent with X1 and X2, based on the 3XMM-DR5 catalog. We also performed an *XMM-Newton* follow-up observation (X3 hereafter, see Table 1) of XJ1417+52 on 2014 January 5. XJ1417+52 was not clearly detected in this observation, and we used it to constrain the long-term evolution of the source.

The source was in the field of view (FOV) of all the three EPIC cameras (i.e., pn, MOS1, and MOS2, Jansen et al. 2001; Strüder et al. 2001; Turner et al. 2001) in the imaging mode in both X1 and X2, but in X3, only MOS1 and MOS2 were collecting science data. We used SAS 14.0.0 to analyze the observations. We first reprocessed the X-ray event files with the calibration files of 2015 July. We excluded the data in strong background flare intervals following the SAS thread for the filtering against high backgrounds, i.e., excluding all intervals when the background exceeded the low and steady level.[15] Short flares were seen in X1 in all cameras, each for $\sim$1% of the time. Flares were absent in X2 in all cameras. Short flares also occurred in X3 in both MOS1 and MOS2, each for 5% of the time. The final clean exposure times used are listed in Table 1. We extracted the source spectra from all available cameras using a circular region of radius 15″, corresponding to a point-spread function (PSF) enclosing fraction of $\sim$70%. The background spectra were extracted from a large circular region of radius 60″–100″ near the source. For the event selection criteria, we used the default values in the pipeline (see Table 5 in Watson et al. 2009). We also created the response files, which were used for spectral fits for X1 and X2 and to estimate the flux for X3. To check the short-term variability in X1 and X2, we extracted the MOS1 background-corrected light curves in the 0.2–1 keV band (negligible counts above 1 keV) and binned at 6 ks using the SAS tool *epiclccorr*. We note that in both X1 and X2 our source was coincident with a dark column in MOS2 and a bright column in pn, resulting in significant loss of counts after filtering out these columns.

Although the 3XMM-DR5 catalog provides an astrometrically corrected position for the source using the Sloan Digital Sky Survey (SDSS) DR9 catalog (Abazajian et al. 2009) as the reference, we double-check the astrometric correction using the deep optical observations of the EGS by the Advanced Camera for Surveys (ACS) Wide Field Camera (WFC) on the *Hubble Space Telescope* (*HST*) and MegaPrime/MegaCam (Boulade et al. 2003) on the Canada–France–Hawaii Telescope (CFHT).

[15] http://xmm.esac.esa.int/sas/current/documentation/threads/EPIC_filterbackground.shtml

Table 1
The X-Ray Observation Log

Obs. ID	Date	Detector	OAA	T (ks)	r_{src}	Count rate (10^{-3} counts s^{-1})	L_{abs} (10^{43} erg s^{-1})	L_{unabs} (10^{43} erg s^{-1})
(1)	(2)	(3)	(4)	(5)	(6)	(7)	(8)	(9)
XMM-Newton:								
0127921001 (X1)	2000 Jul 21	MOS1/MOS2/pn	3.′4	54.8/54.8/44.2	15″/15″/15″	2.5 ± 0.2/1.7 ± 0.2/4.7 ± 0.3	$2.3^{+0.6}_{-0.4}$	$3.8^{+3.1}_{-1.4}$
0127921201 (X2)	2000 Jul 23	MOS1/MOS2/pn	3.′4	18.3/18.3/12.8	15″/15″/15″	2.0 ± 0.3/1.0 ± 0.3/2.3 ± 0.5	$1.9^{+0.9}_{-0.7}$	$2.7^{+8.5}_{-1.1}$
0723860101 (X3)	2014 Jan 05	MOS1/MOS2	1.′7	26.9/26.8	15″/15″	<1.0	<0.7	<1.1
Chandra:								
3305(C1)	2002 Aug 11	ACIS-I0	5.′8	29.1	4.″0			
4357(C2)	2002 Aug 12	ACIS-I0	5.′8	83.7	4.″0	0.14 ± 0.03	$0.5^{+0.4}_{-0.3}$	$0.5^{+0.7}_{-0.2}$
4365(C3)	2002 Aug 21	ACIS-I0	5.′8	83.6	4.″0			
5851(C4)	2005 Oct 15	ACIS-I2	9.′1	35.7	7.″0			
7181(C5)	2005 Oct 15	ACIS-I2	9.′1	16.0	7.″0	< 0.20	<0.6	<1.0
16027(C6)	2014 Sep 15	ACIS-S3	0.′2	26.6	1.″2			
17487(C7)	2014 Oct 11	ACIS-S3	0.′2	32.6	1.″2	<0.10	<0.15	<0.25

Note. Columns: (1) the observation ID with our designation given in parentheses, (2) the observation start date, (3) the detector, (4) the off-axis angle, (5) the exposure times of data used in final analysis, (6) the radius of the source extraction region, (7) the net count rate with 1σ uncertainties or 3σ upper limits (0.2–1 keV for *XMM-Newton* observations, 0.3–1 keV for *Chandra* observations C1–C5 and 0.2–1 keV for *Chandra* observations C6–C7, all in the observer frame; the count rate upper limit for X3 is from the combination of MOS1 and MOS2; we note significant loss of counts in MOS2 and pn in X1 and X2 due to the presence of instrumental bad columns), (8) source rest-frame 0.28–14.2 keV luminosity from the MCD fits, corrected for Galactic absorption but not intrinsic absorption, with 90% uncertainties or 3σ upper limits, (9) source rest-frame 0.28–14.2 keV luminosity from the MCD fits, corrected for both Galactic and intrinsic absorption, with 90% uncertainties or 3σ upper limits. The luminosity upper limits for X3, C4–C5 and C6–C7 were calculated assuming the spectral shape of X1 and have been corrected for PSF loss. All upper limits were calculated with the CIAO task *aprates*, which adopts the Bayesian approach.

We started with the source detections in the 3XMM-DR5 catalog for all five observations in 2000 (i.e., including the three observations not analyzed in detail in this paper). The source detection in the *XMM-Newton* catalog used a maximum likelihood fitting procedure (Watson et al. 2009; Rosen et al. 2015). We first aligned all X-ray observations to the longest observation, i.e., X1, using the astrometric correction method described in Appendix (it is used for all astrometric corrections throughout the paper), using sources with 95% positional uncertainties <2″. The uncertainties of the X-ray positions include both the statistical component and a possible systematic component of 0.″37 (1σ in R.A. and Decl., Rosen et al. 2015). After the relative astrometry correction, the average X-ray source positions weighted by the uncertainties were obtained and then matched to the optical sources in the *HST*/ACS/WFC F814W images from the All-wavelength EGS International Survey (Davis et al. 2007) and the MegaPrime/MegaCam i'-band images from the CFHT Legacy Survey (CFHTLS, Gwyn 2012), which were matched to the SDSS astrometry. Only X-ray sources with 95% positional uncertainties <1″ were used for the astrometric correction; the uncertainties of optical sources should be small and were assumed to be 0.″1 (1σ) in R.A. and Decl. We note that XJ1417+52 was excluded from the matches used for astrometric correction in this step, in order to reduce the effect of the astrometric correction on the identification of its optical counterpart.

2.2. Chandra Observation

XJ1417+52 was in the FOV of seven *Chandra* observations (C1–C7 hereafter; refer to Table 1), all using the imaging array of the AXAF CCD Imaging Spectrometer (ACIS; Bautz et al. 1998). C1–C5 were part of the *Chandra* survey of the EGS (Laird et al. 2009), with C1–C3 taken between 2002 August 11–21 and C4–C5 taken on 2005 October 15. Our source fell in the front-illuminated chip I0 in C1–C3 with an off-axis angle of 5.′8 and in I2 in C4–C5 with an off-axis angle of 9.′1 (near the CCD edge). C6 and C7 were our follow-up observations of the source in 2014 September–October. The aim point was chosen to be at the back-illuminated chip S3 because our source had been ultrasoft. We applied the latest calibration (CALDB 4.6.7) by reprocessing all the data with the script *chandra_repro* in the *Chandra* Interactive Analysis of Observations (CIAO, version 4.7) package. We extracted source and background spectra from circular regions and created the corresponding response matrices for all observations using the script *specextract*. The radii of the source regions in C1–C3, C4–C5, and C6–C7 are 4.″0, 7.″0, and 1.″2 (Table 1), corresponding to PSF enclosing fractions of 90%, 70%, and 95% at 0.6 keV, respectively. We used a source region of a smaller PSF enclosing fraction for observations in which the source has a larger off-axis angle, in order to reduce the background effect, because the PSF of *Chandra* degrades significantly at large off-axis angles. A large background region of radius 30″ was used for all observations. Our source was detected in C1–C3, but not in C4–C7. We used *combine_spectra* to combine the spectra of C1–C3 into a single spectrum for spectral fitting, because these observations are close in time and have very few source counts (the total net source counts are 38 in 0.3–7.0 keV). Similarly we combined the spectra of C4 and C5 into a single spectrum and the spectra of C6 and C7 into another one. These combinations were to put a tighter constraint on the limit of the source flux in these observations, in which our source was not detected.

In order to determine the position of XJ1417+52 from C1–C3, in which the source was weakly detected, we merged these

observations after correcting the relative astrometry between them. The astrometric correction used sources detected with the CIAO wavelet-based source detection tool *wavdetect* (Freeman et al. 2002), which was applied to 0.5–7.0 keV count images binned at the single sky pixel resolution (0.″492). The exposure maps were constructed at the corresponding monochromatic effective energy, i.e., 2.3 keV (Evans et al. 2010). The PSF maps used correspond to the 40% enclosed counts fraction at 2.3 keV. Only sources with 95% positional uncertainties (based on Equation (12) of Kim et al. 2007) <2.″0 were used for astrometric correction. C2 was used as the astrometric reference. New aspect solution files were created from the relative astrometric correction obtained and then applied to the event files for C1 and C3. The CIAO script *merge_obs* was then used to combine the event lists of C1–C3. The source detection was then carried out on the merged observation twice. The first time was on the 0.5–7.0 keV count image to detect sources and align the astrometry to that of optical sources from *HST*/ACS/WFC F814W-band and CFHTLS MegaPrime/MegaCam *i*′-band images, as we did to obtain *XMM-Newton* position of our source. The second time was on the 0.3–1.0 keV count image (the exposure and PSF maps at 0.6 keV were used) to obtain the position of XJ1417+52, considering that our source was ultrasoft. In order to calculate the statistical positional uncertainty for our source, we carried out 2000 ray-trace simulations with *MARX* 5.1.0 at positions near it and at the same off-axis angle. The spectrum from the multicolor disk (MCD) fit to C1–C3 (Section 3.2) was assumed.

2.3. The HST Images

There are two images (in two filters: F606W and F814W) taken by the *HST*/ACS/WFC on 2004 December 15 in the field of our X-ray source. Each image has four frames of 525 s each. As will be shown later in Section 3.1, these images indicate that our source has a candidate host galaxy SDSS J141711.07+522540.8 (GJ1417+52 hereafter) with extent ∼4″ and a very faint candidate optical counterpart (sGJ1417+52 hereafter) at a ∼1″ offset from the nucleus. In order to derive their main photometric parameters, we fitted the *HST*/ACS/WFC images using GALFIT (Peng et al. 2010) with multiple Sérsic components (convolved with the PSF) for the galaxy and a PSF model for the faint optical source, which seems unresolved in these images. In order to improve the statistics, especially for the faint source sGJ1417+5, the fits used 5″ × 5″ (centered at the center of the galaxy) stacked images (one for each filter) from aligned and bundled[16] FLC frames. The effective PSFs[17] at the position of our source in the four frames were averaged and used to fit the stacked images. Because of dithering in the observations, different frames had different degrees of distortion at the position of our source, causing some problem in stacking them. However, we found that the fits to single frames with the corresponding PSFs gave similar results.

2.4. The Gemini Spectroscopic Observation

The galaxy GJ1417+52 was observed during the night of 2013 February 8 (UT) with the Gemini Multi-Object Spectrograph (GMOS, Hook et al. 2004) at the Gemini North Telescope, in queue mode (program ID GN-2013A-Q-37). The data were acquired during dark time (illumination fraction 0.8%), under photometric conditions and ∼0.″70 seeing. The 400 lines/mm ruling density grating (R400) centered at 7000 Å was used. We chose a slit of width 0.″75 and put it through the center of the galaxy GJ1417+52 and the source sGJ1417+52 in order to obtain their spectra simultaneously. A total of four exposures of 1500 s each were obtained. Small offsets in the spectral direction (50 Å) toward the blue and the red were applied between exposures to allow for the gaps between CCDs to avoid any loss of important lines present in the spectra. Spectroscopic flats and comparison lamp (CuAr) spectra were taken after each science exposure. In addition, to derive the sensitivity function and flux calibrate the science spectrum, the spectrophotometric standard star G191B2B was observed as part of the baseline calibration provided by the observation. Because the standard star was observed on a different night (2013 March 03 UT) and under different observing conditions, the science spectrum was calibrated in relative flux.

We processed the observations and extracted the spectrum for the galaxy GJ1417+52 following the standard procedures for long-slit observations provided by the Gemini/GMOS package in IRAF. In summary, the science exposures, comparison lamps and spectroscopic flats were bias subtracted and trimmed. Spectroscopic flats were then processed to remove the calibration unit plus GMOS spectral response, normalizing and leaving only pixel-to-pixel variations and fringing. The bias subtracted, flat fielded two-dimensional science spectra were then wavelength calibrated and rectified (S-shape distortions removed), sky-subtracted, extracted to a one-dimensional format using a fixed aperture of 1.″2 in width around the center of the galaxy, and average combined.

The final spectrum of the galaxy has a resolution of ∼5.5 Å FWHM (measured using sky lines at ∼7000 Å), a dispersion of ∼1.36 Å pixel^{-1}, and a signal-to-noise ratio about 40 at 7000 Å, covering a wavelength interval from ∼4850 to 9180 Å. We identified the most prominent absorption lines (as no clear emission lines were detected) in the spectrum and derived the redshift by employing a line-by-line Gaussian fit using the *rvidline* routine in the IRAF RV package. We fitted the spectrum to multi-component models comprised of single-population synthetic spectra, using Penalized Pixel Fitting (pPXF) software (Cappellari & Emsellem 2004) and Vazdekis et al. (2010) synthetic spectra spanning a grid of 24 ages between 1 to 14 Gyr and six metallicities [M/H] = {−1.71, −1.31, −0.71, −0.40, 0.00, +0.22}.

The source sGJ1417+52 is very faint and has strong contamination from the extended emission of the galaxy, and our Gemini observation is only useful for searching for strong emission lines from it. We followed a method similar to Soria et al. (2013) for ESO 243-49 HLX-1 to obtain a galaxy subtracted spectrum for this source. We first aligned and stacked the sky background subtracted 2D spectra from the four exposures. The galaxy emission was then modeled and subtracted by fitting a third-order cubic spline function along the spatial direction on the northern half of the galaxy, excluding 6 pixels (∼0.″9) centered around sGJ1417+52.

[16] http://stsci.edu/hst/wfc3/documents/ISRs/WFC3-2014-24.pdf
[17] http://stsci.edu/hst/acs/documents/isrs/isr0601.pdf

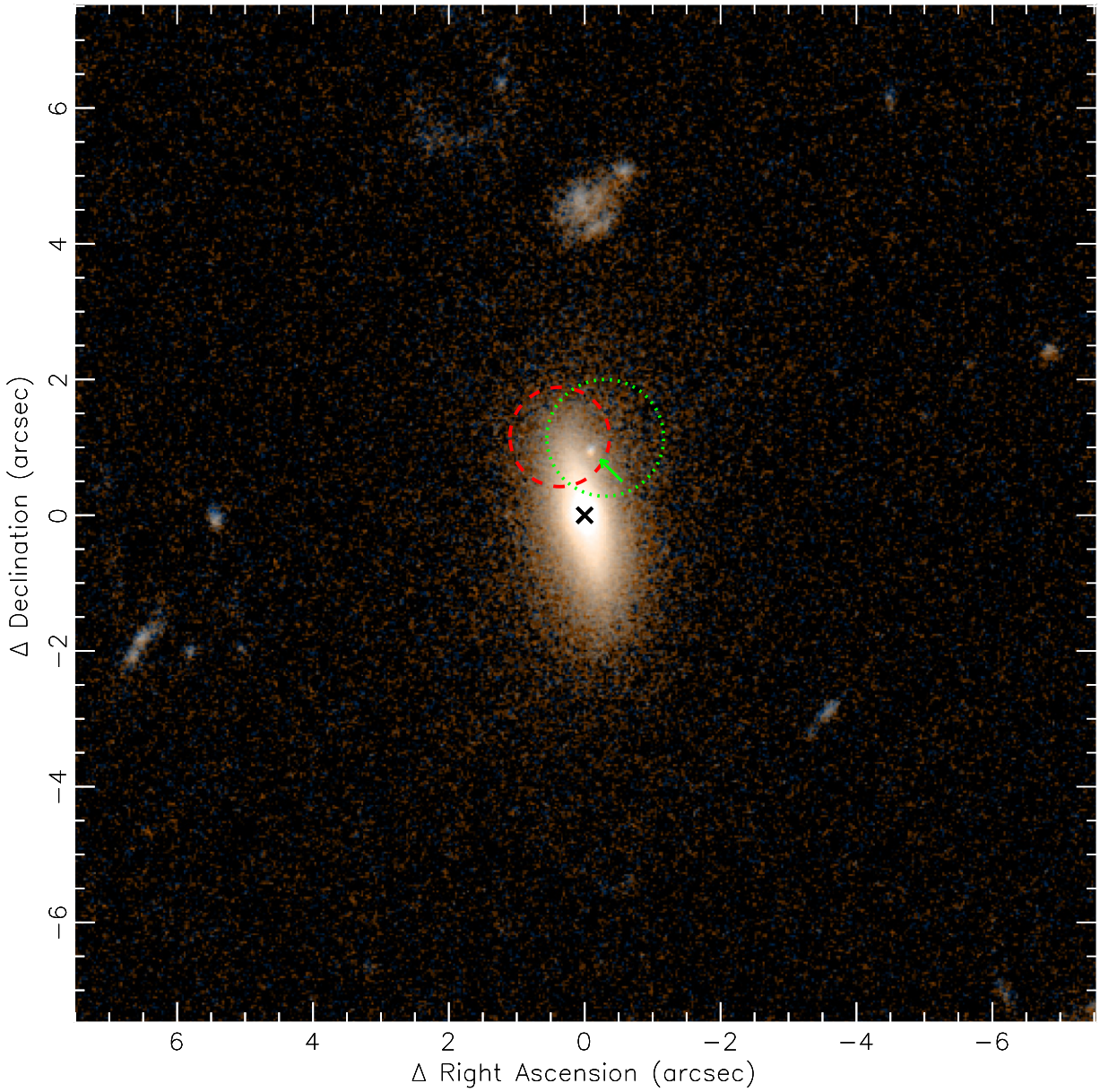

Figure 1. *HST*/ACS/WFC multidrizzled image in the field of XJ1417+52, with the origin at the center of the galaxy GJ1417+52 (black cross, R.A. = 14:17:11.076, Decl.=+52:25:40.80). The angular scale of GJ1417+52 is 5.5 kpc/1″. The image is false-colored, using the F814W (red) and F608W (blue) images and their mean (green). The green arrow points to a faint optical source sGJ1417+52 at R.A. = 14:17:11.066 and Decl.=+52:25:41.74. The 95% positional error (0.″73) of XJ1417+52 from the *XMM-Newton* observations is marked as a red dashed circle, and that (0.″86) from the *Chandra* observations as a green dotted circle, both indicating that the faint optical source could be the counterpart to our X-ray source.

3. RESULTS

3.1. The Source Position and the Environment

The positions of XJ1417+52 that we obtained from the *XMM-Newton* and *Chandra* observations are R.A. = 14:17:11.11, Decl. = +52:25:42.0, and (R.A. = 14:17:11.04, Decl. +52:25:41.9, with the 95% uncertainties of 0.″73 and 0.″86, respectively. They are separated by 0.″67 but are consistent with each other within the uncertainties. The *XMM-Newton* position that we obtained is only 0.″16 from that given in the 3XMM-DR5 catalog, and thus they are also consistent with each other within the uncertainties. We show the *HST*/ACS/WFC F606W and F814W false-colored image in the field of XJ1417+52 in Figure 1, with the X-ray positions above denoted. Our source is close to GJ1417+52, which seems to be an S0 galaxy. However, neither of the X-ray positions is consistent with the galaxy center within the 95% uncertainties. Instead, both X-ray positions are consistent with a faint but clearly visible optical source (i.e., sGJ1417+52, pointed to by a green arrow in Figure 1) in the northern part of the galaxy within the 95% uncertainties. Based on the *HST* observations of the EGS, we calculated the chance probability for our X-ray source to be within ∼1.″0 of the center of a galaxy similar to or brighter than GJ1417+52 in the F814W band to be 0.03%. Similarly, based on the density of optical sources as bright as or brighter than sGJ1417+52 in the F814W band, we calculated the chance probability for sGJ1417+52 to be within ∼1.″0 of our X-ray source is 5%. These probabilities are relatively low and allow us to conclude that XJ1417+52 is most likely in GJ1417+52, with sGJ1417+52 being the optical counterpart.

Table 2
Fitting Results of the *HST*/ACS/WFC Images Around the Field of XJ1417+52

Components[a]	1st Sérsic	2nd Sérsic	3rd Sérsic	PSF
F606W				
Integrated magnitude (AB mag)	21.57 ± 0.01	21.27 ± 0.03	21.62 ± 0.03	26.33 ± 0.04
Effective radius (pixel[b])	1.63 ± 0.02	14.02 ± 0.17	30.97 ± 0.62	···
Index	1.78 ± 0.04	1.01 ± 0.02	0.76 ± 0.04	···
Axis ratio	0.65 ± 0.01	0.25 ± 0.01	0.52 ± 0.01	···
Position angle (degree)[c]	14.95 ± 0.64	13.01 ± 0.11	3.45 ± 1.11	···
F814W				
Integrated magnitude (AB mag)	20.49 ± 0.01	20.48 ± 0.02	20.66 ± 0.02	25.51 ± 0.03
Effective radius (pixel[b])	1.69 ± 0.02	13.48 ± 0.12	28.83 ± 0.34	···
Index	1.71 ± 0.03	0.79 ± 0.02	0.65 ± 0.02	···
Axis ratio	0.58 ± 0.01	0.26 ± 0.01	0.47 ± 0.01	···
Position angle (degree)[c]	15.45 ± 0.41	13.01 ± 0.08	6.17 ± 0.47	···

Notes.
[a] The three Sérsic components were used to fit the galaxy GJ1417+52 (their centers were consistent with each other and were thus forced to be the same in the final fits), and the PSF was used to fit the faint optical source sGJ1417+52.
[b] The pixel scale is 0.″05 (i.e., 0.28 kpc).
[c] The position angle is from the north to the east.

The results of our fits to the *HST*/ACS/WFC images of GJ1417+52 and sGJ1417+52 are given in Table 2. We required three Sérsic components to fit the galaxy, and adding another component did not improve the fit significantly. The fits are good, with no clear large residuals left. We added a PSF model in the fits to check whether a bright point source was present at the galaxy center but saw no significant improvement on the fits either; the central point source, if present, would be ∼4 mag fainter than the galaxy. Based on the sizes, indices, and axis ratios, the first and second Sérsic components in Table 2 are probably the bulge and the disk, respectively. The third one is much larger in size (effective radius $R_e \sim 8$ kpc) and could be a halo. The galaxy has integrated magnitudes of $m_{F606W} = 20.28$ AB mag and $m_{F814W} = 19.35$ AB mag, and the optical source sGJ1417+52 has $m_{F606W} = 26.33$ AB mag and $m_{F814W} = 25.51$ AB mag, thus about 6 mag fainter than the galaxy. To put a constraint on the size of sGJ1417+52, we tried to model it with a Sérsic profile (convolved with the PSF) instead of a single PSF. We assumed an axis ratio of 1.0 and considered two possible indices: $n = 1.0$ and 4.0. The 3σ upper limits of the effective radius R_e were found to be 63 pc and 113 pc for the F606W and F814W bands, respectively, in the case of $n = 1.0$, and were 30 pc and 80 pc, respectively, in the case of $n = 4.0$. The best-fitting R_e values were consistent with zero (i.e., reduced to be a PSF) within 1σ in all cases.

The Gemini spectrum of the galaxy GJ1417+52 is shown in Figure 2. The spectrum exhibits no clear emission lines, but has typical absorption features indicating a passive galaxy at a redshift of $z = 0.41827 \pm 0.00011$ ($D_L = 2.3$ Gpc). We estimated the 3σ upper limit of the flux of [O III] λ5007 to be 3.6×10^{-18} erg s^{-1} cm^{-2}, which corresponds to a luminosity of 2.3×10^{39} erg s^{-1} after Galactic extinction correction. Applying the bolometric correction factors from the [O III] λ5007 flux in Lamastra et al. (2009), we obtained the 3σ upper limit of the bolometric luminosity of the persistent nuclear activity to be 2.0×10^{41} erg s^{-1}. We note that the MMT had spectroscopic follow-up on the X-ray sources in the EGS in 2007–2008, with GJ1417+52 being one of the targets. The spectrum has much lower quality than the Gemini one, with the upper limit of the flux of [O III] λ5007 estimated to be much higher (4.8×10^{-17} erg s^{-1} cm^{-2}, 2σ, Yan et al. 2011), but Coil et al. (2009) obtained a redshift ($z = 0.4184$) consistent with our results.

The pPXF fitting results are shown in Figure 2. The light-weighted age is 8.4 Gyr, while the mass-weighted age is 9.4 Gyr. The total mass is $\sim 4.1 \times 10^{11} M_\odot$, and the total luminosity within the fitting band (source rest-frame 3541–6479 Å) is $\sim 2.8 \times 10^{10} L_\odot$, after rescaling the spectrum to match the integrated F814W flux to correct for the slit loss and the calibration uncertainty.

The fit implied a stellar velocity dispersion of $\sigma_\star \sim 247$ km s^{-1}. Using the relation between M_{BH} and $\sigma_\star$ in Gültekin et al. (2009), we inferred $M_{BH} \sim 4.0 \times 10^8 M_\odot$ (the 1σ uncertainty is 0.31 dex). We also estimated the central BH mass of the galaxy based on the BH mass versus bulge rest-frame *K*-band luminosity relation (Marconi & Hunt 2003; Graham 2007). The *K* band in the source rest frame is approximately the Wide-field Infrared Survey Explorer (WISE) *W*1 band (Wright et al. 2010) in the observer frame for GJ1417+52, which has a magnitude of $m_{W1} = 15.7$ mag ($M_{W1} = -25.7$ mag). Thus we alternatively estimated the BH mass to be $\sim 3.1 \times 10^8 M_\odot$ (the 1σ uncertainty is 0.33 dex), assuming the bulge-to-total luminosity ratio of 35% obtained from the fits to the *HST* F814W image above. The above two estimates of the central BH mass agree with each other very well.

At the redshift of GJ1417+52, the source sGJ1417+52 has a projected offset of ∼5.2 kpc from the nucleus of the galaxy. We did not find any continuum emission, as expected considering that it is so faint, or any significant emission line from its galaxy subtracted 2D spectrum at any wavelength covered by our Gemini observation (∼4850–9180 Å). We fitted its *HST* F606W and F814W photometry with the Maraston (2005) stellar population model that is based on theoretical atmospheres with the Salpeter initial mass function. We adopted this model considering its broad wavelength coverage as needed here. We assumed a single population with a solar metallicity and a Galactic reddening value of $E(B - V) = 0.039$ mag (Schlegel et al. 1998, the intrinsic reddening is neglected considering that the absorption inferred from X-ray spectral fits

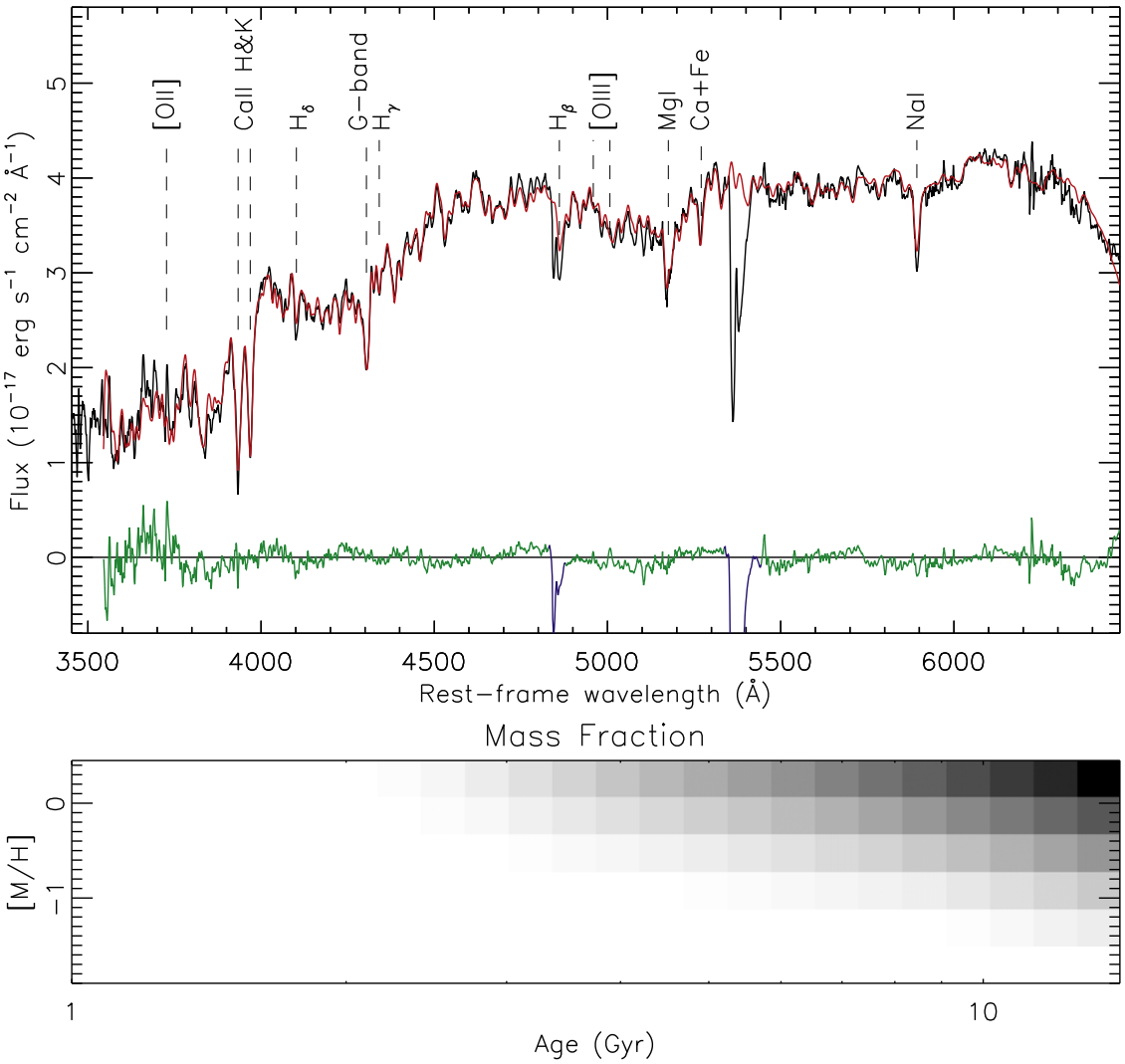

Figure 2. (Upper panel) Relative flux calibrated Gemini spectrum (black) of the host galaxy of XJ1417+52 vs. the source rest-frame wavelength, with the best-fitting pPXF model (red) and residuals (green/blue) overplotted. The two drops at around 4844 Å and 5360 Å (corresponding to 6870 Å and 7604 Å, respectively, in the observer frame; indicated by the blue residuals), are due to the atmospheric OH absorption and were excluded in the fit. The spectrum bluer than 3541 Å was not fitted because the stellar models do not cover this wavelength range. Important stellar absorption and AGN diagnostic emission lines are denoted for reference. For clarity, we have smoothed data points with a boxbar function with width 5 pixels for clarity. (Lower panel) Relative mass fractions of different stellar populations with respect to metallicity and age, with darker shading indicating a larger mass fraction in the best-fitting model.

is consistent with zero). The redshift of $z = 0.41827$ was applied. We inferred a stellar population of age 0.8 Gyr and bolometric luminosity 2.3×10^{42} erg s^{-1} (or $5.9 \times 10^{8}\,L_{\odot}$, corresponding to $5.9 \times 10^{7}\,M_{\odot}$). If we assume a systematic error of 0.1 mag in our derivation of the photometry, the 90% upper limit of the age would be 3 Gyr. Assuming at this age, the bolometric luminosity would be 2.4×10^{42} erg s^{-1} (or $6.4 \times 10^{8}\,L_{\odot}$, corresponding to $7.8 \times 10^{8}\,M_{\odot}$). With photometric information in two filters only, we cannot test multiple stellar population models. Considering that sGJ1417+52 has a F606W−F814W color similar to GJ1417+52, we cannot rule out that sGJ1417+52 contains multiple stellar populations, with mass dominated by old populations.

3.2. X-Ray Spectral Modeling

We carried out spectral fits for X1, X2 and C1–C3. Because of their poor statistics, we rebinned the source spectra to have a minimum of one count per bin and adopted the C statistic to fit the source and background spectra simultaneously. We fitted over the 0.2–10 keV and 0.3–8 keV energy bands for *XMM-Newton* and *Chandra* spectra, respectively. As our source is most likely associated with GJ1417+52 at $z = 0.41827$ (Section 3.1), instead of being a foreground source (see discussion in Section 4), we applied this redshift to the spectral models using the convolution model *zashift* in XSPEC, unless indicated otherwise. All models included the Galactic absorption of $N_{\rm H} = 1.1 \times 10^{20}$ cm^{-2} (Kalberla et al. 2005) using the *tbabs* model. Possible absorption intrinsic to the source was also taken into account using the *ztbabs* model. We used the abundance tables of Wilms et al. (2000). The uncertainties of the parameters from the spectral fits are all at the 90% confidence level throughout the paper.

The X-ray spectra are ultrasoft, with little emission above 1 keV. When we fitted the spectra with a power law (PL), we obtained unphysically high photon indices of $\Gamma_{\rm PL} = 7.5 \pm 1.2$, 7.0 ± 2.1, and $5.3^{+2.2}_{-0.7}$, respectively, implying the thermal origin of the spectra. Therefore, we fitted the spectra with a single-temperature blackbody (BB, *bbodyrad* in XSPEC)

Table 3
Fitting Results of the X1, X2, and C1–C3 Spectra of XJ1417+52

X1		
Models	BB	MCD
$N_{\rm H,i}$ (10^{20} cm^{-2})	$0.0^{+7.4}$	$4.5^{+7.6}$
$kT_{\rm MCD}/kT_{\rm BB}$ (keV)	$0.113^{+0.007}_{-0.014}$	$0.132^{+0.019}_{-0.019}$
$N_{\rm MCD}/N_{\rm BB}$	60^{+127}_{-19}	43^{+124}_{-28}
$L_{\rm abs}$ (10^{43} erg s^{-1})[a]	$2.4^{+0.4}_{-0.5}$	$2.3^{+0.6}_{-0.4}$
$L_{\rm unabs}$ (10^{43} erg s^{-1})[b]	$2.4^{+1.8}_{-0.4}$	$3.8^{+3.1}_{-1.4}$
$L_{\rm bol}$ (10^{43} erg s^{-1})[c]	$3.4^{+3.2}_{-0.6}$	$8.9^{+10.7}_{-3.9}$
C/ν[d]	198.6(194)	197.1(194)
X2		
Models	BB	MCD
$N_{\rm H,i}$ (10^{20} cm^{-2})	$0.0^{+16.4}$	$3.5^{+18.8}$
$kT_{\rm MCD}/kT_{\rm BB}$ (keV)	$0.118^{+0.016}_{-0.025}$	$0.140^{+0.034}_{-0.037}$
$N_{\rm MCD}/N_{\rm BB}$	39^{+351}_{-21}	23^{+433}_{-18}
$L_{\rm abs}$ (10^{43} erg s^{-1})[a]	$1.9^{+0.6}_{-0.6}$	$1.9^{+0.9}_{-0.7}$
$L_{\rm unabs}$ (10^{43} erg s^{-1})[b]	$1.9^{+4.4}_{-0.5}$	$2.7^{+8.5}_{-1.1}$
$L_{\rm bol}$ (10^{43} erg s^{-1})[c]	$2.6^{+7.8}_{-0.8}$	$6.1^{+31.0}_{-3.0}$
C/ν[d]	66.1(78)	66.3(78)
C1–C3		
Models	BB	MCD
$N_{\rm H,i}$ (10^{20} cm^{-2})	$0.0^{+15.8}$	$0.0^{+16.0}$
$kT_{\rm MCD}/kT_{\rm BB}$ (keV)	$0.135^{+0.028}_{-0.024}$	$0.169^{+0.043}_{-0.036}$
$N_{\rm MCD}/N_{\rm BB}$	$4.6^{+18.8}_{-3.6}$	$1.8^{+10.4}_{-1.4}$
$L_{\rm abs}$ (10^{43} erg s^{-1})[a]	$0.4^{+0.3}_{-0.2}$	$0.5^{+0.4}_{-0.3}$
$L_{\rm unabs}$ (10^{43} erg s^{-1})[b]	$0.4^{+0.6}_{-0.2}$	$0.5^{+0.7}_{-0.2}$
$L_{\rm bol}$ (10^{43} erg s^{-1})[c]	$0.5^{+0.8}_{-0.2}$	$1.0^{+1.9}_{-0.5}$
C/ν[d]	36.6(34)	34.8(34)

Note. The C statistic was adopted, and the redshift of $z = 0.41827$ was applied in all fits. All uncertainties are at the 90% confidence level.
[a] Rest-frame 0.28–14.2 keV luminosity, corrected for Galactic absorption but not intrinsic absorption.
[b] Rest-frame 0.28–14.2 keV luminosity, corrected for both Galactic and intrinsic absorption.
[c] The bolometric luminosity based on the total flux of the BB or MCD component.
[d] The C statistic and the degrees of freedom.

model and an MCD model (*diskbb* in XSPEC). The fitting results are given in Table 3, and the example MCD fits to X1 and C1–C3 are shown in Figure 3. The source rest-frame temperatures are in the range of $kT_{\rm BB} \sim 0.11$–0.14 keV from the BB fits and in the range of $kT_{\rm MCD} \sim 0.13$–0.17 keV from the MCD fits. Although it seems that the best-fitting temperature is a little lower in X1 than in C1–C3 (e.g., $kT_{\rm MCD} = 0.13 \pm 0.02$ keV versus 0.17 ± 0.04 keV), they are consistent within the 90% uncertainties. The slightly higher best-fitting temperature in C1–C3 from the BB and MCD fits could be due to presence of some very weak hard emission above 1 keV in these observations. When we tried to fit X1 and C1–C3 spectra with an MCD plus a PL, with the photon index fixed at 2.0, we obtained a zero PL normalization for X1 and a non-zero PL normalization for C1–C3 but only at the 90% significance level. The best-fitting disk temperature becomes $kT_{\rm MCD} = 0.15 \pm 0.04$ keV for C1–C3, thus closer to that of X1. The strength of the soft excess $R_{\rm exc}$, measured by the ratio of unabsorbed 0.3–2 keV (source rest-frame) flux in the MCD and PL components, is >61 (the 90% lower limit) and ∼34 for X1 and C1–C3, respectively, which are much higher than those

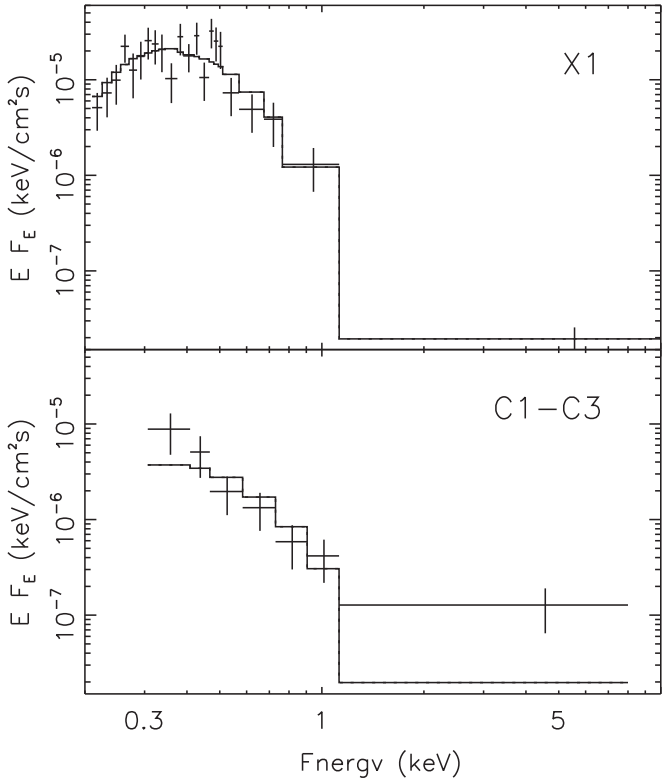

Figure 3. The unfolded spectra of X1 (upper panel, for clarity, only the MOS1 spectrum is shown) and C1–C3 (lower panel) from the MCD fits. For clarity, the spectra were rebinned to be above 2σ per bin in the plot.

of ultrasoft AGNs ($R_{\rm exc} \lesssim 17$, Gierliński & Done 2004). We will describe the source luminosities from these spectral fits in Section 3.3.

For easy comparison with Galactic sources, we also fitted the spectra assuming the X-ray source to be in our Galaxy. Adopting an absorbed BB model, we obtained $kT_{\rm BB} = 79 \pm 8$ eV, 85 ± 14 eV, and 99 ± 18 eV, for X1, X2, and C1–C3, respectively. The corresponding 0.3–10 keV unabsorbed luminosities are $2.8^{+1.1}_{-0.6} \times 10^{30} d^2$ erg s^{-1}, $2.2^{+2.0}_{-0.6} \times 10^{30} d^2$ erg s^{-1}, and $5.2^{+4.3}_{-1.7} \times 10^{29} d^2$ erg s^{-1}, where d is the source distance in units of kpc, respectively. Therefore the source would be very faint if it is in our Galaxy. The best-fitting column densities are $N_{\rm H} = 1.\quad 0^{+2.2} \times 10^{20}$ cm^{-2}, $0.5^{+4.7} \times 10^{20}$ cm^{-2}, and $0.0^{+6.2} \times 10^{20}$ cm^{-2} (the lower error bounds of $N_{\rm H}$ are all zeros), respectively.

3.3. The Long-term and Short-term X-Ray Variability

Figure 4 shows the long-term rest-frame 0.28–14.2 keV (observer-frame 0.2–10 keV) unabsorbed luminosity $L_{\rm X}$ curve of XJ1417+52. The luminosities were obtained based on the MCD fits (Section 3.2) and assuming $D_L = 2.3$ Gpc (Section 3.1); for observations in which the source was not detected, the 3σ upper limits were estimated based on the MCD fit to the X1 spectrum. The source was first detected in X1 and X2 in 2000 July, with $L_{\rm X} = 3.8^{+3.1}_{-1.4} \times 10^{43}$ erg s^{-1} and $2.7^{+8.5}_{-1.1} \times 10^{43}$ erg s^{-1}, respectively. The source was still detected in C1–C3 in 2002 August, with $L_{\rm X} = 0.5^{+0.7}_{-0.2} \times 10^{43}$ erg s^{-1}, a factor of ∼7 lower than that in X1. The source was not detected in C4–C5, X3, and C6–C7, with $L_{\rm X} < 0.9 \times 10^{43}$ erg s^{-1}, $<1.1 \times 10^{43}$ erg s^{-1}, and $<0.25 \times 10^{43}$ erg s^{-1}, respectively. Therefore it appears that

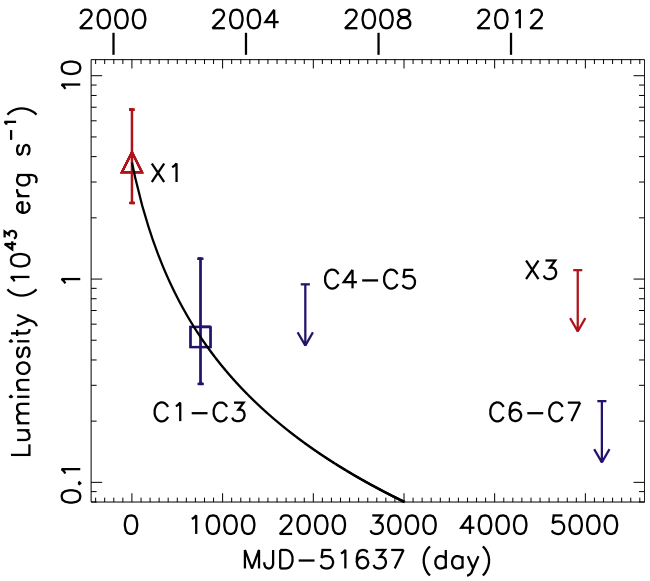

Figure 4. The long-term rest-frame 0.28–14.2 keV unabsorbed luminosity curve, with 90% uncertainties or 3σ upper limits (see Table 1). For clarity, X2 is not plotted because it is only two days after X1 and had a similar luminosity (but with a larger uncertainty). The solid line represents a $(t - t_{\rm D})^{-5/3}$ decline passing through the X1 and C1–C3 data points, which implies the disruption time $t_{\rm D}$ to be ∼11 months before X1.

the source was experiencing an outburst in 2000–2002, with the X-ray luminosity decreasing by a factor of >14 in C6–C7 from X1.

Figure 5 shows the light curves from X1, X2, and C1–C3. The temporal bin sizes used are relatively large (6 ks for X1 and X2 and 28 ks for C1–C3) due to the poor statistics of all observations. Short-term variability might be present in X1 and C2 but is not significant. The probability that the source is not variable is 52% for X1.

4. DISCUSSION

4.1. The Wandering Massive BH Explanation

Both the *Chandra* and *XMM-Newton* positions indicate that our X-ray source XJ1417+52 could be associated with the galaxy GJ1417+52, with an offset of ∼1″ from the galaxy nucleus. Therefore, it is an HLX candidate, with the peak luminosity of $L_X = 3.8 \times 10^{43}$ erg s^{-1} in X1. The source could be an accreting wandering BH of mass $\sim 10^5\,M_\odot$, assuming that it was at the Eddington limit in X1. This mass is around the boundary between IMBHs and SMBHs. The temperature at the inner radius in a standard thin disk at a given Eddington ratio is expected to depend on the BH mass as $M_{\rm BH}^{-1/4}$, and Galactic BHBs tend to have $kT_{\rm MCD} \sim 1$ keV in the bright thermal state (Remillard & McClintock 2006; Done et al. 2007). Therefore, our explanation of the source as a BH of mass $\sim 10^5\,M_\odot$ is supported by its very soft X-ray spectra of $kT_{\rm MCD} \sim$ 0.1–0.2 keV.

Our source has a faint optical counterpart candidate sGJ1417+52. It appears somewhat red in the optical and is thus unlikely to be the emission from accretion activity. It has a rest-frame absolute *V*-band (close to the observer-frame F814W band) magnitude of ∼−15.9 AB mag and is thus much more luminous than globular clusters ($M_V \gtrsim -13$ AB mag, refer to, e.g., Sivakoff et al. 2007). However, it is consistent with a compact dwarf satellite galaxy, which is reminiscent of M32 in M31. It might have been tidally stripped by GJ1417+52, resulting in the remnant nucleus. A possible merging/interacting signature could be that the outer/halo component of GJ1417+52 is a little twisted toward sGJ1417+52, compared with the inner components (by ∼10°; refer to the position angles of all components in Table 2).

Tidally stripped galaxies are often used to explain UCDs and compact elliptical galaxies (cEs) detected in nearby galaxies (Hilker et al. 1999; Drinkwater et al. 2000; Phillipps et al. 2001; Bellovary et al. 2010; Norris et al. 2014; Chilingarian & Zolotukhin 2015; Jennings et al. 2015). UCDs have $R_{\rm e} \lesssim 100$ pc, stellar mass $\lesssim 10^8\,M_\odot$, and $M_V \gtrsim -14.0$ mag, while cEs have $R_{\rm e} \sim$ 100–700 pc, stellar mass $\sim 10^8$–$10^{10} M_\odot$, and M_V from ∼ −14 to −20 mag (e.g., Norris et al. 2014). With $R_{\rm e} \lesssim 100$ pc (or larger, considering possible systematic errors due to, e.g., contaminating emission from GJ1417+52), the stellar mass $\sim 6 \times 10^7\,M_\odot$ (or larger if it contains old stellar populations), and $M_V \sim -15.9$ AB mag, sGJ1417+52 is most likely a massive UCD or a cE.

Due to the large distance, we cannot completely rule out that our X-ray source is embedded in a globular cluster that is much smaller than sGJ1417+52 and cannot be detected in the *HST* images. We have viewed sGJ1417+52 as the most likely, interesting counterpart to our X-ray source, because its large size makes it more likely to host a large BH of $\sim 10^5\,M_\odot$.

If XJ1417+52 is really a massive BH embedded in the remnant nucleus of a dwarf satellite galaxy, one explanation for the outburst is the tidal disruption of a surrounding star by the BH. Fundamental theory predicts the mass accretion rate in TDEs to follow a $(t - t_{\rm D})^{-5/3}$ decay, where $t_{\rm D}$ is the disruption time (Rees 1988, 1990). Because our source was only detected in two epochs (2000 July and 2002 August), we cannot test whether its luminosity decay followed this relation. In Figure 4, we plot a $t^{-5/3}$ decay curve that passes through the X1 and C1–C3 data points and implies $t_{\rm D}$ to be ∼11 months before X1. This decay curve predicts much lower fluxes in the observations after C1–C3 than the detection limits, explaining the non-detection of our source in those observations. Hydrodynamical simulations predicted that the mass accretion rate in TDEs might decay faster than $t^{-5/3}$ (Guillochon & Ramirez-Ruiz 2013). The disrupted star is more likely to be a main-sequence star, instead of a white dwarf (WD). This is because WD TDEs require smaller BHs ($\lesssim 10^5\,M_\odot$) for the disruption to be outside the event horizon of the BH and should have much shorter duration (≲1 year, Rosswog et al. 2009) than our event, which appeared to last for more than two years. We note that the known candidate X-ray TDEs are all associated with the nuclei of main galaxies, and our source could be the first X-ray TDE discovered to be in the nucleus of a stripped satellite galaxy. One off-nuclear optical TDE candidate has been reported in Arcavi et al. (2014). Strong narrow emission lines were not detected from sGJ1417+52 in our Gemini observation, which could be because the lines as echoes of the X-ray flare either had decayed significantly a decade after the disruption or were too weak to be detected, as is often the case (Gezari et al. 2003).

Our source had a peak X-ray luminosity one order of magnitude higher than that of ESO 243-49 HLX-1 and two orders of magnitude higher than those of other HLXs. Its distance is also one order of magnitude larger than those of other HLXs (2.3 Gpc for our source versus <200 Mpc for others). Therefore our source could be the most luminous and

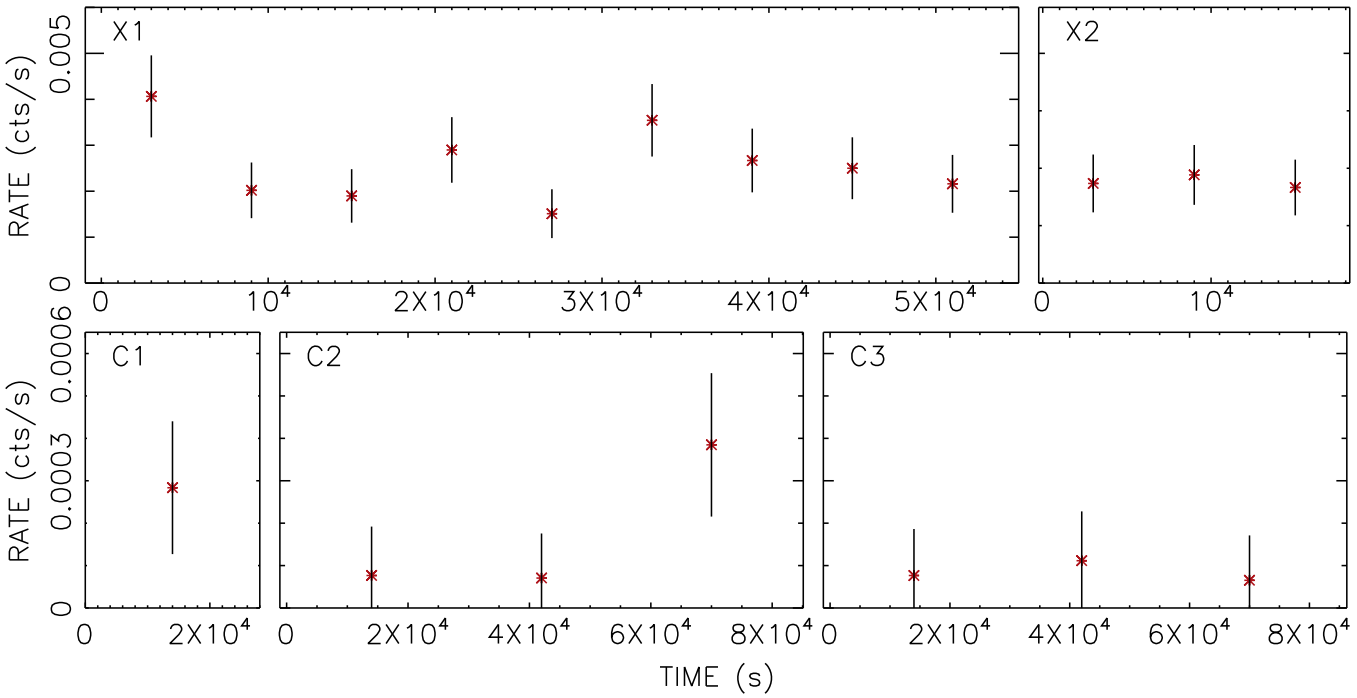

Figure 5. The background subtracted light curves for *XMM-Newton* observations X1 and X2 (upper panels, MOS1 camera, 0.2–1 keV, bin size 6 ks) and for *Chandra* observations C1–C3 (lower panels, 0.3–1 keV, bin size 28 ks). We note that X1 and X2 are separated by two days, while C2 is one day after C1 and C3 is nine days after C2. The 1σ uncertainties are included, and they are calculated following Gehrels (1986) for the *Chandra* observations due to low counts of most data points.

the most distant HLX candidate ever discovered. It is the only HLX candidate other than ESO 243-49 HLX-1 showing very soft X-ray spectra and with an early-type host (both are S0 galaxies). ESO 243-49 HLX-1 also has an optical counterpart, with a projected offset of 3.3 kpc from the nucleus of ESO 243-49, thus similar to our source, but it appeared blue, unlike the optical counterpart to our X-ray sources, which appeared relatively red. The nature of the optical counterpart to ESO 243-49 HLX-1 is still somewhat under debate and could be a very young (∼20 Myr) stellar cluster with a mass of $\sim 10^5\,M_\odot$, with additional contribution from disk irradiation at long wavelengths (Farrell et al. 2012, 2014). The scenario of the remnant nucleus of a bulgy or bulgeless satellite galaxy tidally stripped by ESO 243-49 has also been carefully explored through *N*-body/smoothed particle hydrodynamics simulations (Mapelli et al. 2013a, 2013b). The optical counterpart to our source is much more massive (by about two orders of magnitude) and much older (though still younger than typical red globular clusters) and is more likely to be the remnant nucleus of a tidally stripped bulgy dwarf galaxy. ESO 243-49 HLX-1 showed quasi-periodic (∼1 year) outbursts (Godet et al. 2014), thus unlikely due to complete tidal disruption of a star in a single passage. Our source is consistent with a transient due to a TDE, but with the sparse coverage of the source, we cannot completely rule out the recurrent nature of the source.

4.2. Alternative Explanations

Because of its close proximity to GJ1417+52, the relatively large positional uncertainties of our X-ray source from *Chandra* and *XMM-Newton* observations allow us to rule out that it is due to the nuclear activity (either as a standard AGN or a TDE) in GJ1417+52 only at the 95% confidence level. However, there are other arguments against the explanation as an AGN/TDE at the nucleus of GJ1417+52. We did not identify XJ1417+52 as an AGN (either in GJ1417+52 or in the background) in Lin et al. (2012), because none of the 753 AGNs in that study has X-ray spectra as soft as XJ1417+52. The large long-term variability factor (>14) of XJ1417+52 found here is not common in AGNs either; only 1.5% of the 753 AGNs in Lin et al. (2012) varied by factors of >10. The AGN explanation is also disfavored based on the lack of the [O III] λ5007 in the Gemini spectrum, which indicates little persistent nuclear activity in GJ1417+52, at least two orders of magnitude lower than the peak X-ray luminosity of our source. XJ1417+52 is unlikely a TDE at the nucleus of GJ1417+52 because the central BH of this galaxy is probably too massive ($\gtrsim 10^8\,M_\odot$) to disrupt a solar-type star outside the event horizon (Rees 1988).

The high X-ray luminosities and ultrasoft X-ray spectra, which probably lasted for ≳2 years, make XJ1417+52 unlikely to be the X-ray afterglow of a γ-ray burst (GRB) or a supernova (SN), following similar arguments that we applied to a TDE candidate in Lin et al. (2015). Essentially, X-ray spectra of the afterglows of GRBs and SNs are generally hard, with $\Gamma_{\rm PL} \lesssim 2$ (Immler 2007; Grupe et al. 2013; Levan et al. 2013). Although some ultralong GRBs were discovered to exhibit very soft late-time X-ray spectra (e.g., Piro et al. 2014; Margutti et al. 2015), their hosts normally show intensive star-forming activity (e.g., Levan et al. 2014), while GJ1417+52 is an early-type galaxy. The long duration of XJ1417+52 cannot be explained with the prompt shock breakouts in SNe, which could show soft X-ray spectra (Soderberg et al. 2008) but are expected to be short (less than hours, Nakar & Sari 2012).

Lin et al. (2012) did not identify XJ1417+52 as a coronally active star because it has a 0.2–12 keV maximum flux to the *K*-band flux ratio of $\log(F_{\rm X}/F_{\rm IR}) > -0.65$ (the lower limit was obtained because no counterpart was found in the 2MASS *K*

band), higher than seen in coronally active stars ($\log(F_X/F_{IR}) \lesssim -0.9$ in case of no flares). The X-ray spectra of XJ1417+52 are much softer than seen in stars too. The 0.2–0.5 keV to 0.5–1.0 keV hardness ratio is -0.55 ± 0.04 in X1, significantly lower than values of $\gtrsim 0.3$ seen in stars (Lin et al. 2012). With highly variable ultrasoft X-ray spectra, XJ1417+52 is similar to supersoft X-ray sources (SSSs), most of which are due to nuclear burning of the hydrogen-rich matter on the surface of a WD in the so-called close binary supersoft sources or supersoft novae (Greiner 2000; Kahabka & van den Heuvel 2006). However, such objects are rare, with only a few tens found in our Galaxy (Greiner 2000; Kahabka & van den Heuvel 2006) and the chance to find one within $1''$ of the center of a bright galaxy should be very small. Besides, these objects have luminosities typically $>10^{36}$ erg s^{-1}, while our source has a bolometric luminosity of 6.3×10^{30} erg s^{-1}, based on a BB fit (redshift set to zero) and assuming a distance of 1 kpc. This assumption on the distance is reasonable, given that our source is at a high Galactic latitude of 60°.

5. CONCLUSIONS

We have carried out a detailed study of the ultrasoft X-ray source XJ1417+52, which is a candidate HLX in the S0 galaxy GJ1417+52 at $z = 0.41827$ ($d_L = 2.3$ Gpc) in the EGS with a projected offset of $\sim 1\farcs0$ (5.2 kpc) from the nucleus. It was serendipitously detected in five *XMM-Newton* observations in 2000 July. Two of them (X1 and X2) have enough counts for detailed spectral fits and show very soft spectra that can be fitted with an MCD of $kT_{MCD} \sim 0.13$ keV and $L_X \sim 4 \times 10^{43}$ erg s^{-1} in the source rest frame. It was still detected in three *Chandra* observations (C1–C3) in 2002 August, also exhibiting ultrasoft spectra of $kT_{MCD} \sim 0.17$ keV but at a lower luminosity of $L_X \sim 0.5 \times 10^{43}$ erg s^{-1}. The source was not detected in later observations, with $L_X < 0.9 \times 10^{43}$ erg s^{-1} in C4–C5 in 2005 October, $L_X < 1.\ 1 \times 10^{43}$ erg s^{-1} in X3 in 2014 January, and $L_X < 0.25 \times 10^{43}$ erg s^{-1} in C6–C7 in 2014 September–October. Therefore the source has a long-term variation factor of >14 and is likely a transient with an outburst in 2000–2002. The source has a faint optical counterpart candidate sGJ1417+52, which has $m_{F606W} = 26.33$ AB mag and $m_{F814W} = 25.51$ AB mag in the observer frame in 2004 December, corresponding to the absolute *V*-band magnitude of ~ -15.9 AB mag. All the properties of our source are consistent with a massive BH of mass $\sim 10^5\ M_\odot$ embedded in the remnant nucleus of a satellite galaxy, with the outburst due to tidal disruption of a surrounding star by the BH. Alternative explanations such as a standard AGN in GJ1417+52 and Galactic SSSs are disfavored.

We thank the referee for valuable comments that help improve the paper. Support for this work was provided by the National Aeronautics and Space Administration through *Chandra* Award Number GO4-15087X issued by the *Chandra* X-ray Observatory Center, which is operated by the Smithsonian Astrophysical Observatory for and on behalf of the National Aeronautics Space Administration under contract NAS8-03060. This work is also supported in part by NASA ADAP grant NNX10AE15G and National Science Foundation grant AST-1515084. We thank Chien Y. Peng for valuable advice on the fitting of the galaxy with GALFIT and thank Jay Anderson for providing aligned and bundled FLC frames.

Based on observations obtained with XMM-Newton, an ESA science mission with instruments and contributions directly funded by ESA Member States and NASA.

Based on observations obtained at the Gemini Observatory, which is operated by the Association of Universities for Research in Astronomy, Inc., under a cooperative agreement with the NSF on behalf of the Gemini partnership: the National Science Foundation (United States), the National Research Council (Canada), CONICYT (Chile), the Australian Research Council (Australia), Ministério da Ciência, Tecnologia e Inovação (Brazil) and Ministerio de Ciencia, Tecnología e Innovación Productiva (Argentina).

APPENDIX
ASTROMETRIC CORRECTION

We needed to either align X-ray sources in various observations or align X-ray sources and optical sources. We adopted a two-step method to find the translation and rotation needed for the astrometric correction, assuming that all sources in the reference frame and sources to be aligned have positions and errors known. The first step is to find the translation and rotation that maximize the number of matches N_{max} within the 99.73% (i.e., 3σ) positional uncertainty. The second step is to find the translation and rotation that minimize the reduced χ^2 (χ is defined as the separation of the matches divided by the total positional uncertainty) for $f\ N_{max}$ matches that have the smallest values of χ. Here f represents the percentage of the matches used to calculate the χ^2 and is adopted to exclude possible spurious or bad matches. Bad matches can occur if one or both of the matched sources have bad positions for some reason, like being too close to the CCD edge or being too close to other sources to be resolved well by the detection tool. We have assumed $f = 90\%$ throughout the paper.

The translation and rotation obtained for the astrometric correction have uncertainties, increasing the positional uncertainties of the aligned sources. We estimated the additional positional uncertainties of the aligned sources associated with the astrometric correction procedure, based on 200 simulations. In each simulation, we first simulated the positions of the sources that have matches around the positions of the matches in the reference frame, with positional uncertainties following the combined positional uncertainties from the reference frame and the frame to be aligned. Then the χ^2 minimization for the fN_{max} matches that have the smallest values of χ was repeated. The corrected positions for each source from the simulations are then used to calculate the uncertainty associated with the astrometric correction, which is added to the original positional uncertainty of the source in quadrature.

REFERENCES

Abazajian, K. N., Adelman-McCarthy, J. K., Agüeros, M. A., et al. 2009, ApJS, 182, 543
Arcavi, I., Gal-Yam, A., Sullivan, M., et al. 2014, ApJ, 793, 38
Bachetti, M., Harrison, F. A., Walton, D. J., et al. 2014, Natur, 514, 202
Bachetti, M., Rana, V., Walton, D. J., et al. 2013, ApJ, 778, 163
Baldassare, V. F., Reines, A. E., Gallo, E., & Greene, J. E. 2015, ApJL, 809, L14
Baumgardt, H., Hopman, C., Portegies Zwart, S., & Makino, J. 2006, MNRAS, 372, 467
Baumgardt, H., Makino, J., & Ebisuzaki, T. 2004, ApJ, 613, 1143
Bautz, M. W., Pivovaroff, M., Baganoff, F., et al. 1998, Proc. SPIE, 3444, 210
Bellovary, J. M., Governato, F., Quinn, T. R., et al. 2010, ApJL, 721, L148
Boulade, O., Charlot, X., Abbon, P., et al. 2003, Proc. SPIE, 4841, 72
Cappellari, M., & Emsellem, E. 2004, PASP, 116, 138

Chilingarian, I., & Zolotukhin, I. 2015, Sci, 348, 418
Coil, A. L., Georgakakis, A., Newman, J. A., et al. 2009, ApJ, 701, 1484
Davis, M., Guhathakurta, P., Konidaris, N. P., et al. 2007, ApJL, 660, L1
Donato, D., Cenko, S. B., Covino, S., et al. 2014, ApJ, 781, 59
Done, C., Gierliński, M., & Kubota, A. 2007, A&AR, 15, 1
Drinkwater, M. J., Jones, J. B., Gregg, M. D., & Phillipps, S. 2000, PASA, 17, 227
Ebisuzaki, T., Makino, J., Tsuru, T. G., et al. 2001, ApJL, 562, L19
Evans, I. N., Primini, F. A., Glotfelty, K. J., et al. 2010, ApJS, 189, 37
Farrell, S. A., Servillat, M., Gladstone, J. C., et al. 2014, MNRAS, 437, 1208
Farrell, S. A., Servillat, M., Pforr, J., et al. 2012, ApJL, 747, L13
Farrell, S. A., Webb, N. A., Barret, D., Godet, O., & Rodrigues, J. M. 2009, Natur, 460, 73
Feng, H., & Soria, R. 2011, NewAR, 55, 166
Freeman, P. E., Kashyap, V., Rosner, R., & Lamb, D. Q. 2002, ApJS, 138, 185
Gehrels, N. 1986, ApJ, 303, 336
Gezari, S., Halpern, J. P., Komossa, S., Grupe, D., & Leighly, K. M. 2003, ApJ, 592, 42
Gierliński, M., & Done, C. 2004, MNRAS, 349, L7
Godet, O., Lombardi, J. C., Antonini, F., et al. 2014, ApJ, 793, 105
Godet, O., Plazolles, B., Kawaguchi, T., et al. 2012, ApJ, 752, 34
Graham, A. W. 2007, MNRAS, 379, 711
Greiner, J. 2000, NewA, 5, 137
Grupe, D., Nousek, J. A., Veres, P., Zhang, B.-B., & Gehrels, N. 2013, ApJS, 209, 20
Guillochon, J., & Ramirez-Ruiz, E. 2013, ApJ, 767, 25
Gültekin, K., Richstone, D. O., Gebhardt, K., et al. 2009, ApJ, 698, 198
Gürkan, M. A., Freitag, M., & Rasio, F. A. 2004, ApJ, 604, 632
Gwyn, S. D. J. 2012, AJ, 143, 38
Heida, M., Jonker, P. G., & Torres, M. A. P. 2015, MNRAS, 454, L26
Hilker, M., Infante, L., Vieira, G., Kissler-Patig, M., & Richtler, T. 1999, A&AS, 134, 75
Hook, I. M., Jørgensen, I., Allington-Smith, J. R., et al. 2004, PASP, 116, 425
Hopman, C., Portegies Zwart, S. F., & Alexander, T. 2004, ApJL, 604, L101
Immler, S. 2007, in AIP Conf. Ser. 937, Supernova 1987A: 20 Years After: Supernovae and Gamma-Ray Bursters, ed. S. Immler, K. Weiler, & R. McCray (Melville, NY: AIP), 246
Islam, R. R., Taylor, J. E., & Silk, J. 2003, MNRAS, 340, 647
Jansen, F., Lumb, D., Altieri, B., et al. 2001, A&A, 365, L1
Jennings, Z. G., Romanowsky, A. J., Brodie, J. P., et al. 2015, ApJL, 812, L10
Kahabka, P., & van den Heuvel, E. P. J. 2006, in Super-Soft Sources, ed. W. H. G. Lewin, & M. van der Klis (Cambridge: Cambridge Univ. Press), 461
Kalberla, P. M. W., Burton, W. B., Hartmann, D., et al. 2005, A&A, 440, 775
Kim, M., Kim, D.-W., Wilkes, B. J., et al. 2007, ApJS, 169, 401
Komossa, S. 2012, EPJWC, 39, 2001
Komossa, S. 2015, JHEAp, 7, 148
Kormendy, J., & Richstone, D. 1995, ARA&A, 33, 581
Laird, E. S., Nandra, K., Georgakakis, A., et al. 2009, ApJS, 180, 102
Lamastra, A., Bianchi, S., Matt, G., et al. 2009, A&A, 504, 73
Lemons, S. M., Reines, A. E., Plotkin, R. M., Gallo, E., & Greene, J. E. 2015, ApJ, 805, 12
Levan, A. J., Read, A. M., Metzger, B. D., Wheatley, P. J., & Tanvir, N. R. 2013, ApJ, 771, 136
Levan, A. J., Tanvir, N. R., Starling, R. L. C., et al. 2014, ApJ, 781, 13
Lidskii, V. V., & Ozernoi, L. M. 1979, SvAL, 5, 16
Lin, D., Maksym, P. W., Irwin, J. A., et al. 2015, ApJ, 811, 43
Lin, D., Webb, N. A., & Barret, D. 2012, ApJ, 756, 27
Lin, D., Webb, N. A., & Barret, D. 2014, ApJ, 780, 39
Liu, F. K., & Chen, X. 2013, ApJ, 767, 18
Liu, J.-F., Bregman, J. N., Bai, Y., Justham, S., & Crowther, P. 2013, Natur, 503, 500
MacLeod, M., Goldstein, J., Ramirez-Ruiz, E., Guillochon, J., & Samsing, J. 2014, ApJ, 794, 9
MacLeod, M., Trenti, M., & Ramirez-Ruiz, E. 2015, ApJ, 819, 70
Madau, P., & Rees, M. J. 2001, ApJL, 551, L27
Maksym, W. P., Lin, D., & Irwin, J. A. 2014, ApJL, 792, L29
Maksym, W. P., Ulmer, M. P., Eracleous, M. C., Guennou, L., & Ho, L. C. 2013, MNRAS, 435, 1904
Mapelli, M., Annibali, F., Zampieri, L., & Soria, R. 2013a, A&A, 559, A124
Mapelli, M., Annibali, F., Zampieri, L., & Soria, R. 2013b, MNRAS, 433, 849
Maraston, C. 2005, MNRAS, 362, 799
Marconi, A., & Hunt, L. K. 2003, ApJL, 589, L21
Margutti, R., Guidorzi, C., Lazzati, D., et al. 2015, ApJ, 805, 159
McClintock, J. E., & Remillard, R. A. 2006, in Compact Stellar X-ray Sources, ed. W. Lewin, & M. van der Klis (Cambridge: Cambridge Univ. Press)
Middleton, M. J., Miller-Jones, J. C. A., Markoff, S., et al. 2013, Natur, 493, 187
Middleton, M. J., Sutton, A. D., Roberts, T. P., Jackson, F. E., & Done, C. 2012, MNRAS, 420, 2969
Motch, C., Pakull, M. W., Soria, R., Grisé, F., & Pietrzyński, G. 2014, Natur, 514, 198
Nakar, E., & Sari, R. 2012, ApJ, 747, 88
Norris, M. A., Kannappan, S. J., Forbes, D. A., et al. 2014, MNRAS, 443, 1151
Pasham, D. R., Strohmayer, T. E., & Mushotzky, R. F. 2014, Natur, 513, 74
Peng, C. Y., Ho, L. C., Impey, C. D., & Rix, H.-W. 2010, AJ, 139, 2097
Phillipps, S., Drinkwater, M. J., Gregg, M. D., & Jones, J. B. 2001, ApJ, 560, 201
Piro, L., Troja, E., Gendre, B., et al. 2014, ApJL, 790, L15
Poutanen, J., Lipunova, G., Fabrika, S., Butkevich, A. G., & Abolmasov, P. 2007, MNRAS, 377, 1187
Ramirez-Ruiz, E., & Rosswog, S. 2009, ApJL, 697, L77
Rees, M. J. 1988, Natur, 333, 523
Rees, M. J. 1990, Sci, 247, 817
Reines, A. E., Greene, J. E., & Geha, M. 2013, ApJ, 775, 116
Reines, A. E., Sivakoff, G. R., Johnson, K. E., & Brogan, C. L. 2011, Natur, 470, 66
Remillard, R. A., & McClintock, J. E. 2006, ARA&A, 44, 49
Rosen, S. R., Webb, N. A., Watson, M. G., et al. 2015, A&A, in press (arXiv:1504.07051)
Rosswog, S., Ramirez-Ruiz, E., & Hix, W. R. 2009, ApJ, 695, 404
Schlegel, D. J., Finkbeiner, D. P., & Davis, M. 1998, ApJ, 500, 525
Servillat, M., Farrell, S. A., Lin, D., et al. 2011, ApJ, 743, 6
Seth, A. C., van den Bosch, R., Mieske, S., et al. 2014, Natur, 513, 398
Sivakoff, G. R., Jordán, A., Sarazin, C. L., et al. 2007, ApJ, 660, 1246
Soderberg, A. M., Berger, E., Page, K. L., et al. 2008, Natur, 453, 469
Soria, R., Hau, G. K. T., & Pakull, M. W. 2013, ApJL, 768, L22
Stone, N., & Loeb, A. 2012, MNRAS, 422, 1933
Strüder, L., Briel, U., Dennerl, K., et al. 2001, A&A, 365, L18
Sutton, A. D., Roberts, T. P., Gladstone, J. C., & Walton, D. J. 2015, MNRAS, 450, 787
Sutton, A. D., Roberts, T. P., Walton, D. J., Gladstone, J. C., & Scott, A. E. 2012, MNRAS, 423, 1154
Turner, M. J. L., Abbey, A., Arnaud, M., et al. 2001, A&A, 365, L27
Vazdekis, A., Sánchez-Blázquez, P., Falcón-Barroso, J., et al. 2010, MNRAS, 404, 1639
Vesperini, E., McMillan, S. L. W., D'Ercole, A., & D'Antona, F. 2010, ApJL, 713, L41
Walton, D. J., Harrison, F. A., Grefenstette, B. W., et al. 2014, ApJ, 793, 21
Watson, M. G., Schröder, A. C., Fyfe, D., et al. 2009, A&A, 493, 339
Webb, N., Cseh, D., Lenc, E., et al. 2012, Sci, 337, 554
Wilms, J., Allen, A., & McCray, R. 2000, ApJ, 542, 914
Wright, E. L., Eisenhardt, P. R. M., Mainzer, A. K., et al. 2010, AJ, 140, 1868
Yan, R., Ho, L. C., Newman, J. A., et al. 2011, ApJ, 728, 38